5-2005

Optimal Flux Weakening in Surface PM Machines Using Fractional-Slot Concentrated Windings

Ayman M. EL-Refaie

Thomas M. Jahns

IEEE Transactions on Industry Applications, Vol. 41, No. 3 (May-June 2005): 790-800. DOI.

Optimal Flux Weakening in Surface PM Machines Using Fractional-Slot Concentrated Windings

A.M. El-Refaie
Department of Electrical and Computer Engineering, University of Wisconsin, Madison, WI
T.M. Jahns
Department of Electrical and Computer Engineering, University of Wisconsin, Madison, WI

Abstract:

A design approach is presented for achieving optimal flux-weakening operation in surface permanent-magnet (SPM) synchronous machines by properly designing the machine's stator windings using concentrated, fractional-slot stator windings. This technique makes it possible to significantly increase the machine inductance in order to achieve the critical condition for providing wide speed ranges of constant-power operation. The conditions for optimal flux weakening can be achieved while simultaneously delivering sinusoidal line-to-line back-electromotive-force waveforms and low cogging torque. A closed-form analytical model is described that

can be used to design SPM machines to achieve optimal flux-weakening conditions. This technique is applied to design a 6-kW SPM machine that achieves constant-power operation over a wide speed range. Performance characteristics of this machine are compared using both closed-form and finite-element analysis.

SECTION I. Introduction

Surface permanent-magnet (SPM) synchronous machines have generally been considered to be poor candidates for achieving wide ranges of constant-power operation by means of flux weakening [1]. The principal reason for this reputation can be found by considering the characteristic current of an SPM machine, defined as

$$I_{\text{ch}} \equiv \frac{\Psi_m}{L_d} \text{Arms}$$

(1)

where Ψ_m is the rms magnet flux linkage and L_d is the d-axis inductance (equal to the q-axis inductance for SPM machines).

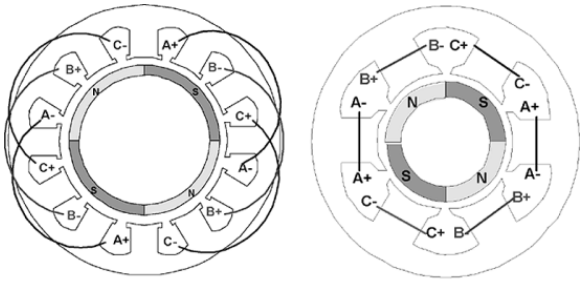

Fig. 1. Comparison of basic stator winding configurations. (a) Distributed with $\text{SPP} = 1$. b) Concentrated winding with $\text{SPP} = 0.5$.

It is well known that the condition for optimal flux weakening in an SPM machine occurs when the machine characteristic current equals the rated current (i.e., $I_{\text{ch}} = I_R$ where I_R is the rated current of the machine) [1], [2]. Unfortunately, the inductance values of SPM machines are typically low with conventional stator winding designs because the permanent magnets mounted on the rotor surface behave as large air gaps in the machine's magnetic circuit. Furthermore, there is limited opportunity to lower the magnet flux linkage Ψ_m in SPM machines without degrading the machine's torque production capability. As a result, the characteristic current values for SPM machines tend to be significantly higher than the rated current, causing severe limits on the machines' constant-power speed range during flux-weakening operation.

The purpose of this paper is to present a design approach for achieving optimal flux-weakening operation in SPM machines by properly designing the machine's stator windings using concentrated, fractional-slot stator windings. Concentrated windings refer to windings that encircle a single stator tooth, eliminating any end-winding overlap with other phase windings. Fig. 1 shows a comparison between conventional distributed and concentrated windings. The term “fractional slot” in this paper refers to stator windings with slot-per-phase-per-pole (SPP) values less than one.

This concentrated fractional-slot winding technique makes it possible to significantly increase the machine inductance in order to reduce the characteristic current to the point of establishing equality with the rated current. It will be shown that the conditions for optimal flux weakening can be achieved while simultaneously delivering near-sinusoidal back-electromotive-force (EMF) waveforms and low cogging torque. Additional

advantages of the approach will be discussed including opportunities for segmented stator construction and the desirable limiting of short-circuit fault current amplitudes.

While other authors have reported on the use of concentrated windings in PM machines [3]–[4][5], there has been no previous publication that describes specific design techniques for applying such windings to achieve optimal flux-weakening conditions in SPM machines. Reference [6] describes an SPM machine equipped with fractional-slot concentrated windings that achieves a wide constant-power speed ratio (CPSR). However, few details are provided to explain the underlying theoretical principles for achieving this performance or how it can be replicated in new designs. In addition, the SPP value selected for this particular machine is nonoptimal since it results in unbalanced radial force acting on the rotor.

In the commercial literature, manufacturers such as ZF Sachs have claimed to achieve wide ranges of constant-power operation using SPM machines [7]. However, no accompanying technical details have been provided to explain how this has been accomplished.

A major objective of this paper is to provide a clear explanation of how concentrated fractional-slot windings make it possible to achieve optimum flux-weakening performance in SPM machines. A systematic machine design procedure based on closed-form analytical techniques is introduced for achieving this desired performance characteristics. The results of applying this design approach to a 6-kW SPM machine are presented to demonstrate that optimal flux weakening can be achieved over a wide (10 : 1) constant-power speed range.

SECTION II.Concentrated Windings and Flux Weakening

The most common stator winding configurations used in SPM machines are as follows:

1. distributed integral-slot windings, among which the one-slot/pole/phase configuration shown in Fig. 1(a) is very popular, especially in the case of brushless dc machines;
2. concentrated fractional-slot windings, among which the 0.5-slot/pole/phase shown in Fig. 1(b) is the most popular.

Concentrated windings offer some significant advantages over distributed windings. These include: 1) significant reduction in the copper volume and copper losses in the end region; 2) significant reduction in the machine total length [3], [4]; 3) reduction in machine manufacturing cost; and 4) compatibility with segmented stator structures that makes it possible to achieve significantly higher slot fill factor values [8], [9].

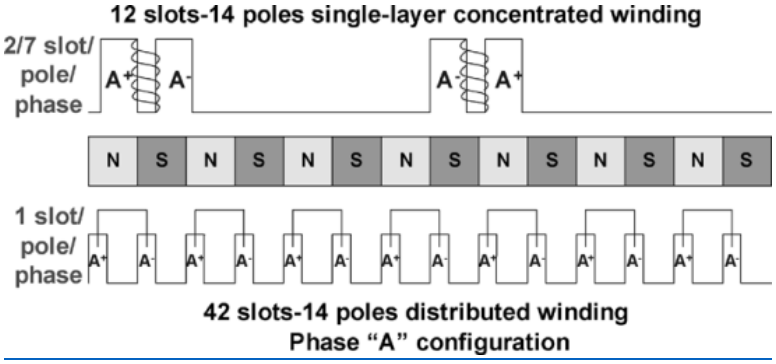

Fig. 2. Comparison of fractional-slot concentrated and distributed full-pitch windings.

Another major advantage that will be explained in this section is that concentrated windings provide higher inductance compared to distributed windings for the same magnet flux linkage. This is the fundamental reason

why concentrated windings have the potential to significantly improve the flux-weakening capabilities of SPM machines.

A. Choice of SPP Value

It has been shown that there are several SPP values in the fractional-slot category that can support concentrated windings [3], [4]. However, different SPP values can result in very different machine characteristics. It is very important to select the SPP values that can achieve the highest machine performance. The criteria for choosing the preferred SPP values have been identified by various authors [3], [4], [10] and are summarized here.

- The winding factor for the spatial frequency that matches the rotor magnet fundamental spatial frequency (henceforth referred to as simply the synchronous frequency) should be as high as possible. This leads to high effective numbers of turns and, hence, lower current for the same torque.
- The lowest common multiple (LCM) of the number of stator slots (S) and the number of rotor poles (2P) should also be as high as possible. The harmonic frequency that corresponds to this LCM order value represents the cogging torque frequency. As a result, choosing SPP values to increase this LCM value raises the cogging torque frequency and lowers its magnitude.
- The greatest common divisor (GCD) of the product of the number of stator slots and the number of rotor poles must be an even number. This GCD value is an indication of the machine's symmetry. If it is an even number, the net radial force on the machine will be very low.

In addition to these established criteria, it is also desirable to choose an SPP value that can support single-layer concentrated windings (i.e., one stator phase coil occupying each slot). Only certain SPP values are compatible with single-layer windings [3], [4]. One advantage of single-layer stator windings is that they are easier to fabricate than double-layer windings that have two phase coils sharing each slot.

More relevant to the topic of this paper, single-layer stator windings create subharmonic spatial flux components (i.e., subharmonics of the synchronous frequency) that are larger than those for double-layer windings. These subharmonic flux components are valuable because they contribute leakage inductance terms that increase the total phase inductance, helping to decrease the value of the characteristic current (1) in order to achieve wide speed ranges of constant-power operation.

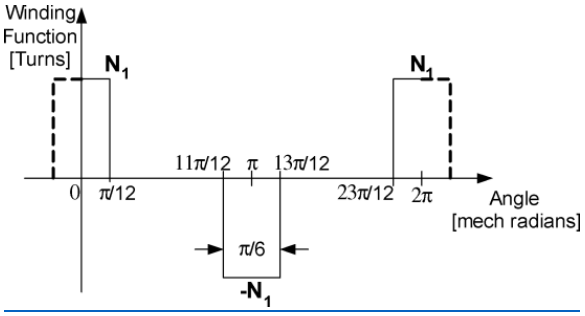

Fig. 3. Winding function of the 12-slot/14-pole concentrated fractional-slot winding design ($\mathrm{SPP} = 2/7$).

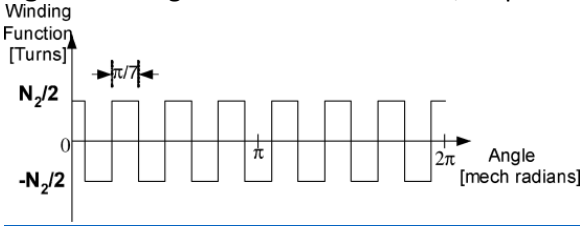

Fig. 4. Winding function of the 42-slot/14-pole distributed winding design ($\mathrm{SPP} = 1$).

Based on this combination of criteria, two families of stator windings corresponding to SPP values of 2/5 and 2/7 emerge as the best candidates. Both of these SPP values are capable of delivering comparable performance, but attention in this paper will be focused on stator windings in the $SSP = 2/7$ family. The resulting analysis and arguments made for the $\mathrm{SPP} = 2/7$ stator windings can be easily extended to the family of stator windings with $SPP = 2/5$.

B. Comparison of Concentrated Fractional-Slot and Distributed Windings

The basic machine stator-rotor repeating unit of the $\mathrm{SPP} = 2/7$ family has 12 stator poles and 14 rotor poles. In order to quantitatively explain why concentrated windings have potential for improving the flux-weakening capabilities of SPM machines, the 12-slot/14-pole single-layer design ($\mathrm{SPP} = 2/7$) will be compared to a distributed 42-slot/14-pole design ($\mathrm{SPP} = 1$) having the same rotor structure.

The phase "A" winding configuration of both designs is shown in Fig. 2. It can be seen that there is a significant difference between the two designs. Over the 14 rotor poles, phase "A" of the 12-slot/14-pole design (designated) has two coils occupying four slots in contrast to seven coils occupying 14 slots in the case of the 42-slot/14-pole design (Winding 2).

The goal of this comparison is to show that *for the same magnet flux linkage*, the concentrated fractional-slot winding configuration provides significantly higher phase inductance compared to the distributed winding configuration. By increasing the inductance, the characteristic current (1) is decreased, making it possible to achieve the conditions for optimum flux-weakening operation.

C. Winding Analysis for Equal Magnet Flux Linkage

The first step is to impose the constraint of equal magnet flux linkage for both windings. It is assumed that the 12-slot/14-pole concentrated winding has N_1 turns/coil while the 42-slot/14-pole distributed winding has N_2 turns/coil. Plots of the two winding functions are provided in Figs. 3 and 4. The magnet flux linkage can be calculated using the winding function method as follows [11]:

$$\Psi_a = r_g l_{\mathrm{eff}} \int_0^{2\pi} N_a(\theta) B(\theta) d\theta \ \mathrm{Wb} - \mathrm{turns}$$

(2)

where

Ψ_a	phase "A" magnet flux linkage (Wb);
r_g	air-gap radius (m);
l_{eff}	active length of the machine (m);
N_a	phase "A" winding function (turns);
B	air-gap magnet flux density (T);
θ	angle along the air-gap periphery (mechanical radians).

For simplicity, it is assumed in this analysis that the magnet flux density is sinusoidal without harmonics. Since it is assumed that both winding designs have the same rotor structure as shown in Fig. 2, the magnet B field will be the same in both designs.

$$B(\theta) = B_{max} \sin(7\theta) \mathrm{T}.$$

(3)

The magnet flux linkage can now be evaluated for each winding.

Winding #1: 12-slot/14-pole concentrated winding (*$\mathbf{SPP} = \mathbf{2/7}$*)

$$\Psi_{a1} = r_g l_{\text{eff}} * \frac{4}{p} K_{w1} N_1 B_{max} \text{Wb} - \text{turns}$$

(4)

where K_{w1} is the fundamental (synchronous) winding factor that has a value of 0.966 for $\text{SPP} = 2/7$ [3], [4], [12].

Winding #2: 42-slot/14-pole distributed winding (*$\mathbf{SPP} = \mathbf{1}$*)

$$\Psi_{a2} = r_g l_{\text{eff}} * 2 N_2 B_{max} \text{Wb} - \text{turns}.$$

(5)

Equating (4) and (5), the relationship between the number of turns per coil needed in the two windings to insure equality of the magnet flux linkage can be determined

$$N_1 = \frac{p}{2K_{w1}} N_2 = 3.623 * N_2.$$

(6)

D. Inductance Calculations

The inductances for the two windings can next be calculated using the winding functions [11]

$$L_{aa} = \frac{\mu_0 r_g l_{\text{eff}}}{g} \int_0^{2\pi} N_a^2(\theta) d\theta \text{ H}$$

$$L_{ab} = \frac{\mu_0 r_g l_{\text{eff}}}{g} \int_0^{2\pi} N_a(\theta) N_b(\theta) d\theta \text{ H}$$

(7)(8)

where

L_{aa}	self-inductance of phase "A" (H);
L_{ab}	mutual inductance between phases "a" and "B" (H);
μ_0	permeability of air (H/m);
g	air-gap thickness (m);
L_d	d-axis inductance [11] =$L_{aa} + L_{ab}$ (H).

The inductances can be evaluated for both windings.

Winding #1: 12-slot/14-pole concentrated winding (*$\mathbf{SPP} = \mathbf{2/7}$*)

$$L_{aa} = \frac{\mu_0 r_g l_{\text{eff}}}{g} N_1^2 \frac{\pi}{3} L_{ab} = L_{ac} = 0\text{H}$$

$$\therefore L_{d-\text{conc}} = \frac{\mu_0 r_g l_{\text{eff}}}{g} N_1^2 \frac{\pi}{3}\text{H}.$$

(9)(10)

Winding #2: 42-slot /14-pole distributed winding (*$\mathbf{SPP = 1}$*)

$$L_{aa} = \frac{\mu_0 r_g l_{\text{eff}}}{g} N_2^2 \frac{\pi}{2} \quad L_{ab} = \frac{Laa}{3}\text{H}$$

$$\therefore L_{d-\text{dist}} = \frac{\mu_0 r_g l_{\text{eff}}}{g} N_2^2 \frac{2\pi}{3}\text{H}.$$

(11)(12)

Combining (6), (8), and (9), the ratio of the d-axis inductances for the two windings under the constraint of equal magnet flux linkage can be evaluated to be

$$\frac{L_{d-\text{conc}}}{L_{d-\text{dist}}} = \frac{N_1^2}{2N_2^2} = 6.56.$$

(13)

This is a very important result because it indicates that for the same magnet flux linkage, replacing a distributed winding ($\text{SPP} = 1$) with a concentrated fractional-slot winding ($\text{SPP} = 2/7$) increases the d-axis inductance by a factor of 6.56. Consequently, the characteristic current of the machine (I_{ch}) is reduced by the same factor, making it much more practical to satisfy the optimum flux-weakening condition of $I_{\text{ch}} = I_R$.

It should be noted that the calculated inductances using winding functions only represent the magnetizing and harmonic leakage inductances. The slot leakage and end leakage inductances are not included. Available evidence indicates that inclusion of these additional leakage inductance components will not change the basic conclusion that concentrated fractional-slot windings offer major advantages for increasing the machine inductance values.

E. Analysis of Inductance Harmonic Components

One approach to achieving a better understanding of what causes the significant increase of inductance values for concentrated windings is to analyze the spatial harmonic spectrum of the winding functions for both the distributed and concentrated windings. The same Windings 1 and 2 used in the preceding inductance calculations are used here. In order to simplify the analysis, the number of turns per coil for the concentrated winding is set to 1 (i.e., $N_1 = 1$). Based on (6), the value of N_2 for the distributed winding is set to 1/3.623 so that the windings satisfy the constraint of equal magnet flux linkage.

The results of performing Fourier spatial harmonic decompositions on both winding functions are plotted in Fig. 5 as a function of spatial harmonic order (i.e., number of cycles per 2π mechanical radians). The same scaling is used for the spatial harmonic spectra of both windings along the horizontal axis so that harmonic components with the same spatial frequency appear at the same position along the horizontal axis.

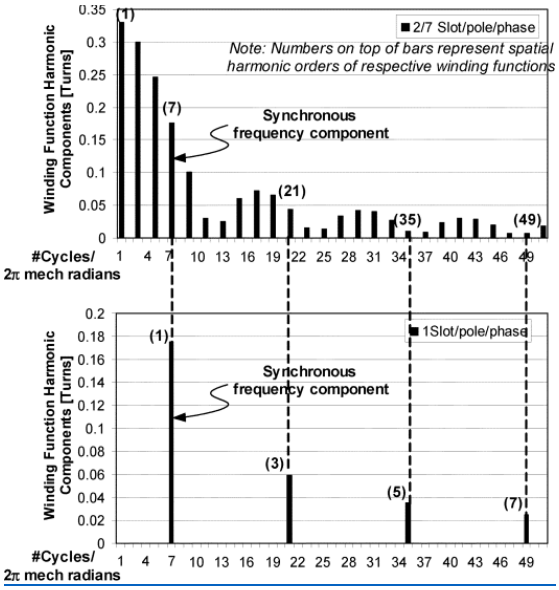

Fig. 5. Spatial harmonic spectra of the winding functions plotted versus spatial frequency (cycles per 2π mechanical radians) for (a) 12-slot/14-pole concentrated winding ($N_1 = 1$) and (b) 42-slot/14-pole distributed winding ($N_2 = 1/3.623$).

One of the first important features to note in Fig. 5 is that the fundamental spatial frequency component of the distributed winding (#2) falls at the same spatial frequency as the seventh spatial harmonic frequency component of the concentrated winding (#1). These two components fall at the synchronous frequency defined by the rotor magnet flux density distribution in (3), and they are the only winding function components that contribute to torque production. Both of these components have the same amplitude because of the equal magnet flux constraint that was imposed. The inductance values associated with these synchronous frequency components comprise the magnetizing inductances of the two windings.

All of the other spatial harmonic components of the two winding functions that do not fall at the synchronous spatial frequency contribute only leakage inductance to their windings. For the concentrated winding, there are three winding function components falling at subharmonics of the synchronous frequency that exceed the amplitude of the synchronous frequency component. In fact, summing all of the inductance components together reveals that the magnetizing inductance of the concentrated winding represents only 9.26% of the phase inductance, with harmonic leakage inductance making up all the rest of the total.

In contrast, the synchronous frequency component is the dominant component in the winding function spatial frequency spectrum for the distributed winding. As a result, the magnetizing inductance associated with this synchronous frequency component comprises approximately 80% of the total phase inductance for the distributed winding.

Thus, the big advantage that the concentrated winding (#1) enjoys over the distributed winding (#2) in terms of higher inductance can be attributed to the much higher harmonic leakage inductance that is developed by the concentrated winding.

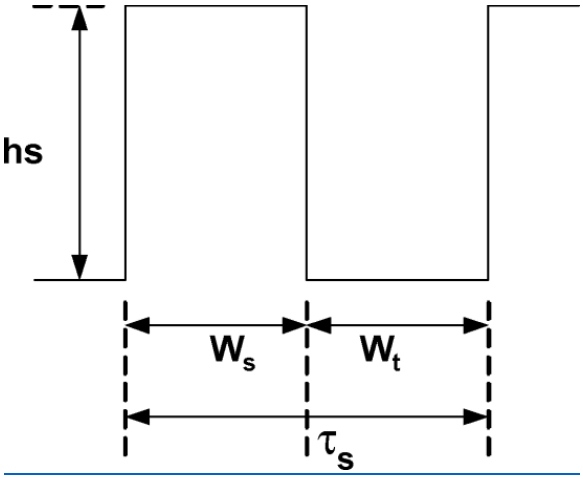

Fig. 6. Key dimensions defining one stator slot pitch of the machine.

The large spatial harmonic components in the winding function associated with the concentrated winding can also create problems because of the harmonic magnetic flux density (B) components that they contribute. The presence of these additional flux density components must be carefully considered during the machine design process in order to minimize their impact on magnetic saturation of the iron core as well as eddy-current losses. Various techniques are available for minimizing these undesirable effects, but such topics fall beyond the scope of this paper.

F. Torque Production

The torque developed by an SPM machine can be expressed as [11]

$$T_e = \frac{3}{2}\frac{P}{2}\Psi_m i_{qs}^r \mathrm{N}\cdot\mathrm{m}$$

(14)

where P is the number of stator poles, and i_{qs}^r is the component of stator current that is spatially oriented in quadrature with the magnet flux axis.

Since the magnet flux linkages of the concentrated and distributed windings are constrained to be equal, the torque developed by the two machine windings for the same amount of stator current (appropriately aligned along the q axis in quadrature with the magnet flux) will also be equal.

G. Current Density

Another performance metric for the concentrated and distributed stator windings that is useful to compare is the stator winding current density. The current density value is important because it plays a large role in determining the maximum current that the stator windings can handle (hence, the maximum torque) before the winding reaches its thermal limit.

The maximum allowable current density value varies based on the type of cooling that is available to the machine, the machine size, and type of enclosure. Hence, this analysis here will focus on the relative values of the current densities in the two stator windings rather than their absolute values.

Fig. 6 shows one slot pitch of the machine. To simplify the analysis, it will be assumed that both the tooth and the slot have uniform widths. Although this is only an approximation due to slot tapering, the fundamental result is not affected since this tapering applies equally to both windings.

The stator winding current density can be calculated as follows:

$$J_a = \frac{I_a}{A_{\text{cond}}} \frac{\text{A}}{\text{m}^2}$$

$$A_{\text{cond}} = \frac{W_s * h_s * K_s}{n_{\text{cond}}} \text{m}^2$$

$$W_s = \lambda_s * \tau_s \text{m}$$

$$\lambda_s = \frac{W_s}{W_s + W_t}$$

(15)(16)(17)(18)

where

J_a	phase "A" current density (A/m);
I_a	phase "A" rms current (A);
A_{cond}	cross-sectional area of one conductor (m^2);
W_s	slot width (m);
W_t	tooth width (m);
h_s	slot height (m);
K_s	slot fill factor (percentage of slot area filled with conductor);
τ_s	slot pitch (m).

For purposes of this analysis, the value of λ_s is set at 0.5 which is a typical value for many ac machines. The slot fill factor is assumed to be 40% for both windings, representative of high-quality random-wound stator windings. The value of the slot height h_s is assumed to be the same with both windings.

Winding #1: 12-slot-/14-pole concentrated winding (*$\mathbf{SPP = 2/7}$*)

$$\tau_s = \frac{\pi}{6} r_s \text{ m}$$

(19)

where r_s is the stator inner radius (m)

$$J_{a1} = \frac{I_a N_1}{(\frac{\pi}{6} r_s) * 0.5 * h_s * 0.4} \frac{\text{A}}{\text{m}^2}.$$

(20)

Winding #2: 42-slot/14-pole distributed winding (*$\mathbf{SPP = 1}$*)

$$\tau_s = \frac{\pi}{21} r_s \text{m}$$

$$J_{a2} = \frac{I_a N_2}{(\frac{\pi}{21} r_s) * 0.5 * h_s * 0.4} \frac{\text{A}}{\text{m}^2}.$$

(21)(22)

Using (6), (20) and (22):

$$\frac{J_{a1}}{J_{a2}} = \frac{N_1 * 0.4 * 6}{N_2 * 0.4 * 21} = 1.036.$$

(23)

This is another significant result. Assuming the same stator current and the same magnet flux linkage in both windings, the current density is almost the same for the concentrated and distributed windings. Even though the concentrated winding has a higher number of turns per stator slot, each stator slot in the concentrated winding is larger in area than a stator slot in the distributed winding because there are fewer slots (12 versus 42). In the end, these two factors nearly cancel each other, leading to nearly the same value of current density for both windings.

Based on the assumptions made in this section, the total slot area available with the concentrated and distributed windings is virtually identical. This occurs because the concentrated winding has 2/7 times the number of stator slots compared to the distributed winding, but each stator slot is 7/2 times the width of the distributed winding slot. Assuming the same fill factor for both windings, this means that both windings have the same wire cross section. Furthermore, the total number of stator windings in the two windings is nearly identical since the concentrated winding has ~3.6 times the number of turns/coil as the distributed winding, but only 1/3.5 times the number of coils, leading to a total turns ratio of 3.623/3.5 = 1.035 for the two windings.

It is worth noting here that concentrated windings are compatible with segmented stators that break the stator into individual stator tooth poles [7]–[8][9]. Segmented stator poles make it possible to wind the solenoidal windings much more tightly than it is possible to do with conventional stator laminations. In fact, other investigations have shown that it is possible to achieve high slot fill factors exceeding 70% using segmented stators, nearly double the values that can be achieved with high-quality distributed windings. This advantage can be used to increase the power density and/or the machine efficiency using concentrated windings.

H. Winding Resistance Calculation

Some attention has also been devoted in this investigation to comparing the stator winding resistances of the distributed and concentrated windings. Unfortunately, this comparison is more complicated than the ones developed for the previous metrics because there are more variables that influence the final result. For example, the details of the end winding design for the distributed windings can have a significant impact on the phase resistance values.

Space limitations in this paper make it impractical to provide a through discussion of the derivation of the resistance values and the impact of key machine design variables. However, it can be stated that analytical results show that the phase resistance values for the two types of stator windings are generally comparable for the same stator slot fill factor.

As discussed in the preceding section on current density, the introduction of a segmented stator structure makes it possible to significantly increase the slot fill factor. Fitting more copper conductor into each slot makes it possible to reduce the resistance of the concentrated winding in order to improve the machine efficiency or torque/power density as noted above.

I. Losses

Special attention must be devoted to the calculation of hysteresis and eddy-current losses in concentrated fractional-winding SPM machines because of the substantial subharmonic components that exist in the air-gap magnetic flux density distribution. Iron loss models are available [16] to provide good estimates of the stator and rotor iron core losses, including the effects of these harmonics.

However, special measures may be required to reduce the eddy-current losses in the rotor magnets induced by the rich harmonic content of the air gap flux distribution. The eddy-current losses in the magnets depend on the choice of magnet material and how the magnets are constructed (e.g., sintered or bonded). In addition, segmentation of the magnets along the air-gap periphery can be very effective in reducing the eddy-current losses [17]. A detailed discussion of the magnet eddy-current losses and techniques for reducing such losses goes beyond the objectives of this paper and will be addressed separately [18].

SECTION III. SPM Machine Design for Optimal Flux Weakening

A. Closed-Form Analytical Model

The first step in designing an SPM machine to achieve optimum flux weakening using concentrated fractional-slot stator windings is to choose the optimum SPP. This step has already been discussed in Section II, leading to preferred SPP values of 2/7 or 2/5.

Machines with concentrated windings pose special challenges to closed-form analysis since the winding distribution deviates significantly from a standard sinusoidal distribution. As a result, classical analytical techniques including dq, complex vector, and ac phasor techniques lose accuracy because their underlying assumptions that require a sinusoidal winding distribution are violated.

A complete closed-form analytical model has been developed for SPM machines equipped with concentrated fractional-slot windings that is valuable for both machine design and performance analysis. The outlines of this design approach are presented here, but space limitations make it necessary to reserve a detailed discussion of the design techniques for a separate paper.

The adopted analytical approach is based on established techniques for calculating the air-gap field distribution including the impact of spatial harmonics in the rotor magnet field distribution and stator slots [14]. The model is sufficiently versatile to handle a wide range of concentrated fractional-slot winding configurations. Calculated quantities include machine back EMF, phase inductance and resistance, as well as average and ripple torque components.

The SPM machine model is configured to calculate the machine both below the corner speed (i.e., constant torque region) and above the corner speed (flux-weakening region). Below the corner point speed when the current regulators are fully active, the program calculates the optimum current waveforms to minimize the torque ripple using current profiling techniques [15]. At elevated speeds in the flux-weakening regime when the current regulators are saturated, frequency-domain analysis is employed to predict the phase current waveforms resulting from six-step voltage excitation.

An iron loss model [16] is incorporated into the analysis that is capable of assessing the impact of higher order harmonic currents that flow at elevated speeds in response to the six-step voltage waveforms. Calculation of the machine cogging torque in the absence of stator excitation is also included. This combination of closed-form analytical tools provides a fast and effective method for predicting SPM machine performance and comparing alternative machine designs that incorporate concentrated fractional-slot windings.

It must be noted that magnetic saturation is not accounted for in the present closed-form analytical model. Fortunately, the low permeability of the magnet material tends to prevent magnetic saturation from becoming a significant factor in most SPM machine designs. Furthermore, magnetic saturation tends to become progressively less of an issue at high speeds because flux weakening is acting, as its name suggests, to reduce the amplitude of the magnetic flux density in the machine.

B. SPM Machine Design Process Using Analytical Model

Many of the steps in designing this type of SPM machine are the same as those used for any other type of ac machine. These machine design techniques are well documented in the literature [19], [20] and will not be repeated here. However, one critical design step that is necessary to achieve optimum flux weakening in the SPM machine deserves discussion here. In particular, a deterministic means has been developed for calculating the magnet remanence (B_r) and the number of series turns (N_s) in the stator winding. Since these two parameters play critical roles in determining the flux-weakening capability of the machine, the means of determining their values must be addressed.

The approach to setting B_r and N_s focuses on the machine parameters Ψ_m and L_d that determine the machine's characteristic current and, hence, its flux-weakening capabilities. A simplified version of the closed-form formula [14] for the magnet flux linkage is presented as follows:

$$\Psi_m = \frac{\sqrt{2}B_1 r_s l_{\text{eff}} N_s K_{w1} \lambda_o}{p} = \frac{k_1 B_r N_s}{p} \text{Wb} - \text{turns}$$

(24)

where B_1 is the peak fundamental component of the air-gap magnet flux density distribution [14], λ_o is the average value of the permeance function to account for the effect of the stator slots, p is the number of pole pairs, and k_1 is a machine constant. Although (24) does not include the impact of harmonics, it represents a very good approximation since the choice of $\text{SPP} = 2/7$ leads to flux linkage and back-EMFwaveforms that are quite sinusoidal (i.e., low harmonic content) as will be shown in Section IV. As a result, the machine can be excited with sinusoidal current waveforms in order to achieve very good performance characteristics.

The inductance model includes both magnetizing and leakage inductances. The total stator winding inductance is proportional to the square of the series stator turns ($L_d \propto N_s^2$), leading to the following proportionality relationship for the characteristic current, using (24):

$$I_{\text{ch}} = \frac{\Psi_m}{L_d} = \frac{k_2 B_r N_s}{p N_s^2} = \frac{k_2 B_r}{p N_s} \text{Arms}$$

(25)

where k_2 is a machine design constant incorporating the machine dimensions and configuration.

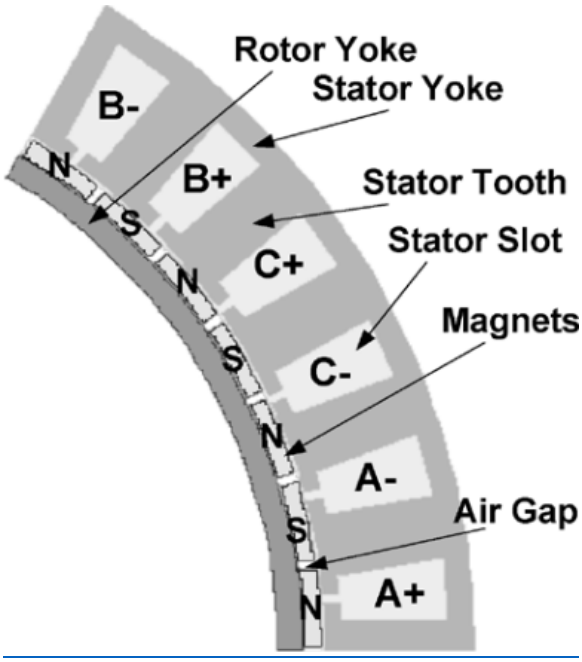

Fig. 7. Basic stator–rotor repeating unit of 6-kW SPM machine for S/A application consisting of six stator slots and seven poles.

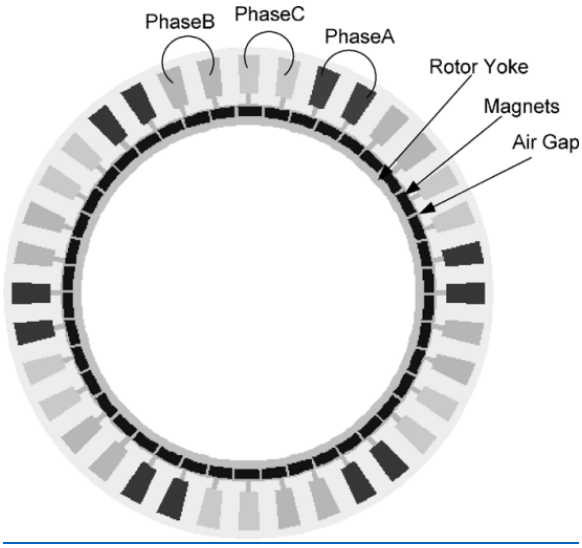

Fig. 8. Cross section of complete 6-kW SPM machine with 36 slots and 42 poles.

The two unknown variables B_r and N_s can be uniquely determined from the two machine design constraints associated with the characteristic current value and the desired corner-point frequency ω_c (electrical rad/s). Assuming that the dimensions of the machine are already determined, the required values of B_r and N_s to achieve optimal flux weakening can be calculated by simultaneously solving the following two equations:

$$\frac{k_2 B_r}{pN_s} = I_R \text{Arms}$$

$$V_s = \sqrt{(\omega_c \Psi_m)^2 + (\omega_c L_d I_R)^2} \text{Vrms}$$

(26)(27)

where V_s is the maximum fundamental rms phase voltage available to the machine (Vrms).
Equation (27) neglects the stator resistance voltage drop that is typically negligible for elevated rotor speeds.

SECTION IV. SPM Machine Design Example

To test this SPM machine concept using concentrated fractional-pole windings, an exercise was launched to design an SPM machine to meet a set of performance requirements that were derived from those of a 6-kW automotive direct-drive starter/alternator (S/A) that had been previously established [13]

The requirements were modified to require nearly constant-power operation *as a motor* over a 10 : 1 speed range extending from 600 r/min (4-kW mechanical output power) to 6000 r/min (6-kW output power).

A machine configuration in the $\mathrm{SPP} = 2/7$ family consisting of 36 slots and 42 poles was chosen for this design exercise. Applying the analytical design tools described in the preceding section, an SPM machine was designed having the basic stator-rotor unit illustrated in Fig. 7, consisting of seven rotor pole magnets facing six stator slots and three concentrated stator windings (one for each of the three phases). Six repetitions of this basic unit around the periphery of the machine are needed to comprise the complete 36-slot/42-pole configuration. Fig. 8 shows a cross section of the complete machine.

A. SPM Machine Performance Characteristics

Table I summarizes key machine dimensions and parameters for the SPM machine designed for the S/A application. The most important observation is that the machine characteristic current is almost exactly equal to the rated current (110 Arms), thereby meeting the conditions for optimum flux-weakening operation.

TABLE I Summary of Key SPM Machine Parameters and Design Metrics. (Note: All I and Ψ Variables are rms Quantities)

Slots/pole/phase	2/7	B_r	0.902 [T]
Number of phases	3	Outer diameter	272 [mm]
Number of slots	36	Active length	60[mm]
Pole pairs	21	Total length	73.1 [mm]
Series turns, N	26	Iron	7.1
Turns/coil	26	Copper	3.3
Parallel	6	Magnet	0.87
Slot	70%	Total	9.07
Current	3.8	Shear	2.24
$I\ R$	**110[A]**	Ld	**0.0819 [mH]**
Ψ_m	**9.9[mWb-t]**	$Ich = \Psi m/Ld$	**113 [A]=1.03 IR**

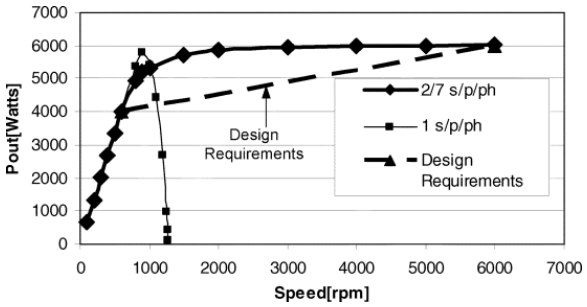

Fig. 9. Calculated power versus speed envelope for the 36-slot/42-pole ($\mathrm{SPP} = 2/7$) and the 36-slot/12-pole ($\mathrm{SPP} = 1$) SPM machines, including S/A performance requirements.

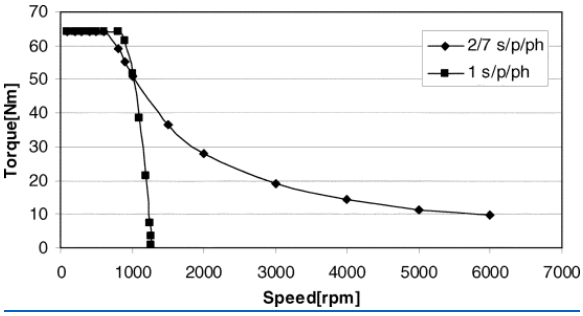

Fig. 10. Calculated torque versus speed envelope for the 36-slot/42-pole ($\mathrm{SPP} = 2/7$) and the 36-slot/12-pole ($\mathrm{SPP} = 1$) SPM machines.

The closed-form analytical tools have been used to predict the SPM machine performance over the full required speed range. The calculated motoring output power vs. speed envelope is provided in Fig. 9, and the output torque vs. speed envelope is presented in Fig. 10. It can be seen that a very wide constant-power speed range is achieved, meeting the design requirements of at least 10 : 1.

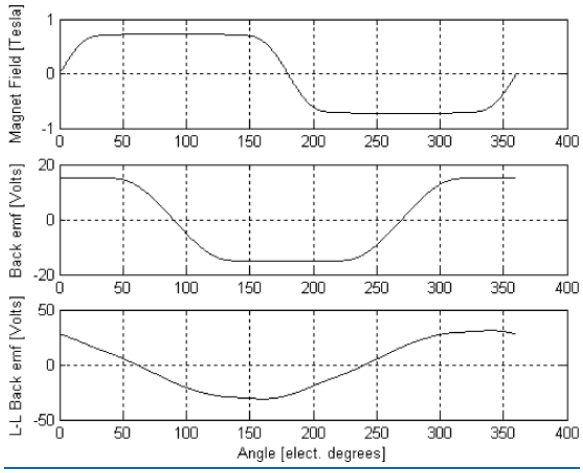

Fig. 11. Calculated air-gap rotor magnet flux density distribution (top) and the corresponding phase-to-neutral (middle) and line-to-line back-EMF (lower) waveforms at 600 r/min.

More specifically, the machine can deliver 4 kW at 600 r/min and 6 kW at 6000 r/min. (The design requirements are shown as a straight line in Fig. 9.)

This result is consistent with the fact that the predicted characteristic current is very close to the rated current value, a condition that would be almost impossible to achieve in an SPM machine using conventional distributed stator windings. To emphasize this contrast, the power and torque versus speed envelopes of a 36-slot/12-pole SPM machine using distributed stator winding ($\mathrm{SPP} = 1$) designed for the same rated torque are overlaid on the corresponding envelopes of the 36-slot/42-pole curves in Figs. 9 and 10. The poor flux-weakening capabilities of the conventional distributed-winding machine are very apparent.

A more detailed performance comparison between interior PM (IPM) machines, SPM machines with concentrated windings, and SPM machines with distributed windings for flux-weakening applications is presented separately [18].

B. Back-EMF Evaluation

The predicted air-gap magnetic flux density distribution produced by the uniformly-magnetized rotor magnets (162 electrical degrees) and the corresponding phase and line-to-line back-EMF waveform at 600 r/min are shown in Fig. 11. It can be observed that the phase-to-neutral back-EMF waveform has higher harmonic content than the line-to-line back EMF. It will be shown below that this difference is caused by a third harmonic voltage component that appears in the phase-to-neutral voltage but disappears automatically in the line-to-line back EMF for wye-connected windings. The relatively low harmonic content of these waveforms may initially be unexpected because of the winding's low SPP value and the presence of significant harmonics components in the air-gap flux density distribution.

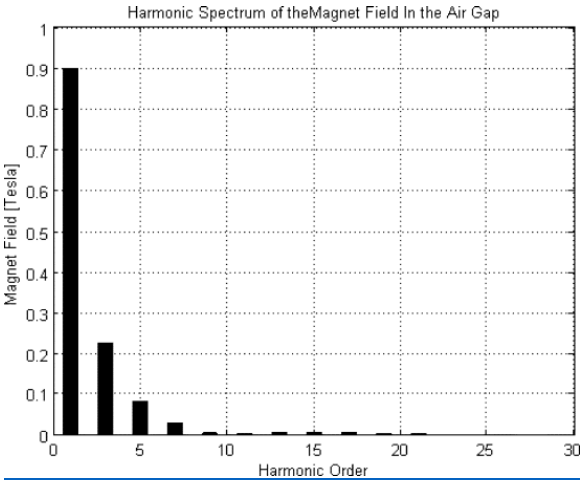

Fig. 12. Predicted spatial harmonic spectrum of the air-gap magnet spatial flux density distribution. The spatial period of the fundamental component for this machine is $2\pi/42$ mechanical radians.

In order to explain this quantitatively, the back EMF e can be expressed in the form of a Fourier series [21]

$$e = \sum_n \omega_r \Phi_n N_s K_{wn} \sin\ np\theta_r = \sum_n E_n \sin\ np\theta_r \text{Vrms}$$

$$\Phi_n = 2B_n r_s l_{\text{eff}} \lambda_o \text{Wbperturn}$$

(28)(29)

where θ_r is the angle between the rotor magnet flux axis and the phase winding axis (mechanical rad), ω_r *(*$=npd\theta_r/dt$) is the rotor angular velocity [electrical rad/s), K_{wn} is the nth harmonic winding factor, and B_n is the magnitude of the nth harmonic component of the air-gap magnet flux density distribution (T).

The harmonic spectrum of the air-gap flux density produced by the magnets is shown in Fig. 12. It can be seen that other than the fundamental component, the only spatial components that have significant values are the third, fifth, and seventh harmonics. The corresponding winding factors for these three harmonics derived for the concentrated fractional-slot stator winding (SPP $= 2/7$) are: $K_{w3} = 0.707$, $K_{w5} = 0.258$, and $K_{w7} = 0.258$. Evaluating (28) with these values shows that even though the fundamental component dominates the phase-to-neutral back-EMF waveform, the third harmonic component causes the waveform to deviate from being purely sinusoidal The resulting total harmonic distortion (THD) of the phase-to-neutral back-EMF voltage is 18%.

As noted above, the third harmonic component is automatically eliminated from the line-to-line back-EMF voltage waveform. Assuming that the wye neutral is floating, the third harmonic component is automatically eliminated from the phase current and instantaneous torque waveforms as well.

C. Cogging Torque Evaluation

One period of the predicted cogging torque of the SPM machine is shown in Fig. 13. The spatial period of the cogging torque waveform is 1.43 mechanical degrees. This result is consistent with the fact that the least common multiple of 36 and 42 is 252, determining the cogging torque spatial frequency.

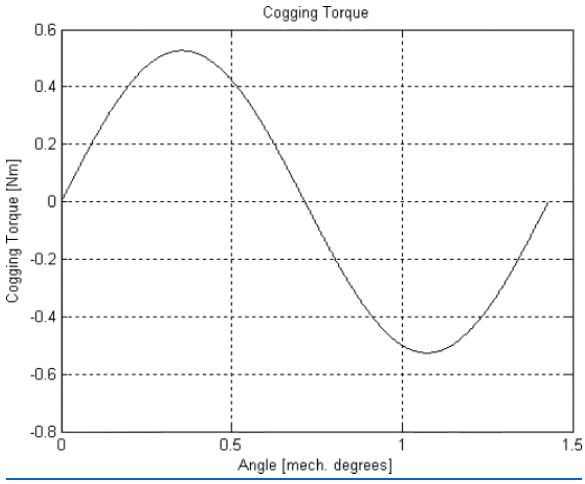

Fig. 13. One period of predicted cogging torque waveform for the 36-slot/ 42-pole SPM machine design.

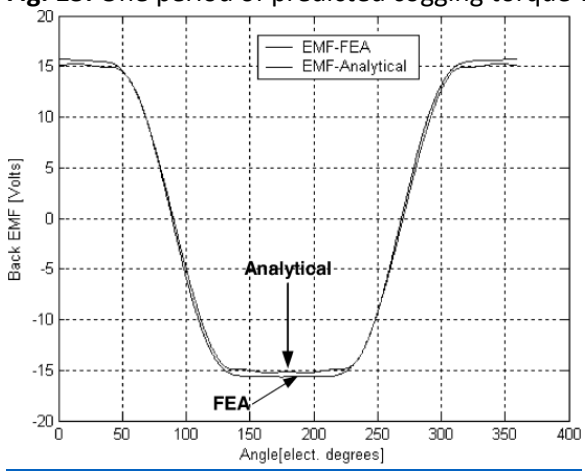

Fig. 14. Phase-to-neutral back-EMF waveforms for the 36-slot/42-pole SPM machine calculated by FEA and closed-form analysis.

The peak-to-peak cogging torque amplitude is approximately 1.5% of the machine rated torque. Such low cogging torque amplitude is consistent with the very high cogging torque frequency attributable to the selected slot/pole combination.

It is worth noting that no special measures were taken in the design to reduce the cogging torque amplitude. If necessary for a particular application, a variety of techniques are available to further attenuate the cogging torque. For example, the magnet span can be adjusted in order to nearly eliminate the lowest frequency component of the cogging torque [22].

SECTION V. Finite-Element Analysis (FEA) Verification

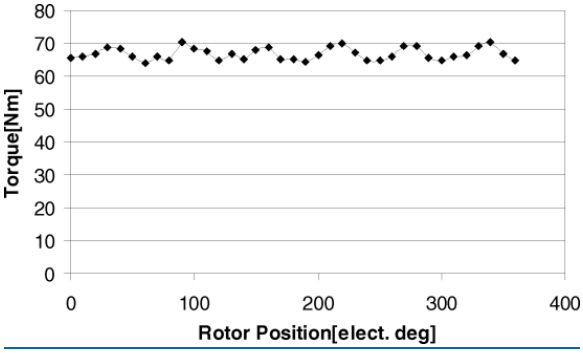

Fig. 15. FEA-calculated torque over one pole pair (360°electrical) for $I = 110$ Arms at 600 r/min with current oriented along the q axis.

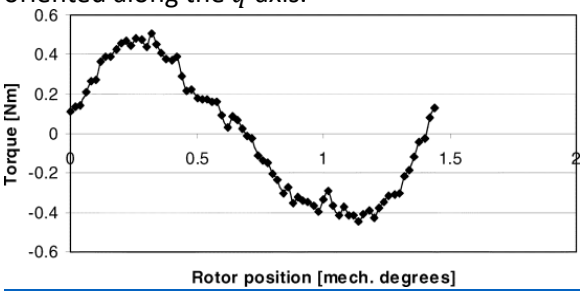

Fig. 16. Predicted cogging torque waveform over one period (1.43 mechanical degrees) using FEA.

FEA has been used to confirm the electromagnetic parameters and performance characteristics of the 36-slot/42-pole SPM machine calculated using the closed-form analytical model. The FEA packages used for this analysis were MagNet 2D by Infolytica and Maxwell 2D by Ansoft.

Fig. 14 shows a comparison of the phase-to-neutral back-EMF waveforms predicted by FEA and closed-form analysis as a function of rotor position at 600 rpm. The difference between the predicted peak fundamental values of Ψ_m derived from the closed-form analysis and FEA is 0.47%, indicating excellent agreement. The corresponding difference in the two predictions of L_d is approximately 7.5%. This error is considered reasonable for this machine because the leakage inductance is very high and difficult to accurately predict.

Fig. 15 shows a plot of the FEA-predicted torque waveform at the machine's corner point speed (600 r/min) with sinusoidal current excitation (no current harmonics). It shows that the machine is capable of producing the required rated torque (64 N·m) during motoring operation at the corner point speed. The torque ripple in the FEA-calculated waveform with sinusoidal excitation is approximately 9% peak to peak. This torque ripple can be further reduced using one of a variety of candidate techniques including current profiling as noted earlier in Section III.

Average torque predictions from the FEA and closed-form analysis also agree within a few percent. Corresponding FEA torque predictions at maximum speed (6000 r/min) confirm the desired 10 : 1 constant-power speed range.

Fig. 16 shows the FEA-predicted cogging torque over one period of 1.43 mechanical degrees, confirming the expected periodicity. In addition, the amplitudes of the predicted cogging torque using FEA and closed-form analysis agree quite well.

Taken together, these FEA results build confidence in the validity of the predictions of the closed-form analytical model. Work is now under way to verify these results experimentally.

SECTION VI. Conclusion

A major conclusion of this paper is that SPM machines can be designed to achieve optimal flux-weakening conditions by introducing concentrated fractional-slot stator windings. A careful technical explanation has been presented describing how concentrated windings achieve this objective by significantly increasing the phase inductance, thereby reducing the machine's characteristic current sufficiently to match its rated current.

A closed-form analytical model has been developed that makes it possible to predict the machine parameters and performance characteristics of SPM machines designed with such windings. Key design steps necessary to achieve optimum flux-weakening conditions have been presented.

The closed-form analytical model has been exercised to develop a design for a 6-kW SPM machine that can deliver constant power over a 10 : 1 speed range by meeting the conditions for optimum flux weakening. FEA has been used to build confidence in the model predictions.

Results of this ongoing research open the door to developing SPM machine designs in a systematic fashion for applications requiring wide speed ranges of constant-power operation that were previously unattainable using conventional distributed windings. Recent results suggest that the concentrated winding technique scales well with machine aspect ratio, number of poles, and machine output power. More complete details of these results and the closed-form analytical model will be presented in separate papers.

ACKNOWLEDGMENT

The authors wish to thank Prof. D. W. Novotny for his many valuable technical discussions. The authors also thank the Wisconsin Electric Machines and Power Electronics Consortium (WEMPEC) for the use of its facilities.

References

1. W. Soong and T. J. E. Miller, "Field weakening performance of brushless synchronous AC motor drives", *Proc. IEĒElect. Power Appl.*, vol. 141, no. 6, pp. 331-340, Nov. 1994.
2. R. F. Schiferl and T. A. Lipo, "Power capability of salient pole permanent magnet synchronous motor in variable speed drive applications", *IEEE Trans. Ind. Appl.*, vol. 26, no. 1, pp. 115-123, Jan./Feb. 1990.
3. J. Cros and P. Viarouge, "Synthesis of high performance PM motors with concentrated windings", *IEEE Trans. Energy Convers.*, vol. 17, no. 2, pp. 248-253, Jun. 2002.
4. F. Magnussen and C. Sadarangani, "Winding factors and joule losses of permanent magnet machines with concentrated windings", *Proc. IEEE IEMDC'03*, vol. 1, pp. 333-339, 2003-Jun.
5. J. Cros, J. R. Figueroa and P. Viarouge, "BLDC motors with surface mounted PM rotor for wide constant power operation", *Conf. Rec. IEEE-IAS Annu. Meeting*, vol. 3, pp. 1933-1940, 2003-Oct.
6. F. Magnussen, P. Thelin and C. Sadarangani, "Performance evaluation of permanent magnet synchronous machines with concentrated and distributed windings including the effect of field weakening", *Proc. PEMD'04*, vol. 2, pp. 679-685, 2004-Mar.-Apr.
7. *ZF Sachs Dynastart Powertrain Systems for Passenger Cars*, 2001, [online] Available: .
8. A. G. Jack, B. C. Mecrow, P. G. Dickinson, D. Stephenson, J. S. Burdess, N. Fawcett, et al., "Permanent magnet machines with powdered iron cores and pressed windings", *IEEE Trans. Ind. Appl.*, vol. 36, no. 4, pp. 1077-1084, Jul./Aug. 2000.
9. H. Akita, Y. Nakahara, N. Miyake and T. Oikawa, "New core structure and manufacturing method for high efficiency of permanent magnet motors", *Conf. Rec. IEEE-IAS Annu. Meeting*, vol. 1, pp. 367-372, 2003-Oct.
10. S. Nishio, *Polyphase direct current motor*, Aug. 1989.
11. D. W. Novotny and T. A. Lipo, Vector Control and Dynamics of AC Drives, U.K., Oxford:Clarendon, 1998.

12. M. M. Liwschitz, "Distribution factors and pitch factors of the harmonics of a fractional-slot winding", *AIEE Trans.*, vol. 62, pp. 664-666, Oct. 1943.
13. E. C. Lovelace, *Optimization of a magnetically saturable interior PM synchronous machine drive*, 2000.
14. Z. Q. Zhu, D. Howe, E. Bolte and B. Ackermann, "Instantaneous magnetic field distribution in brushless permanent magnet DC motors Part I: Open-circuit field", *IEEE Trans. Magn.*, vol. 29, no. 1, pp. 124-135, Jan. 1993.
15. J. Y. Hung and Z. Ding, "Design of currents to reduce torque ripple in brushless permanent magnet motors", *Proc. Inst. Elect. Eng.*, vol. 140, no. 4, pp. 260-266, Jul. 1993.
16. C. Mi, G. R. Slemon and R. Bonert, "Modeling of iron losses of permanent-magnet synchronous motors", *IEEE Trans. Ind. Appl.*, vol. 39, no. 3, pp. 734-742, May/Jun. 2003.
17. K. Atallah, D. Howe, P. H. Mellor and D. A. Stone, "Rotor loss in permanent-magnet brushless AC machines", *IEEE Trans. Ind. Appl.*, vol. 36, no. 6, pp. 1612-1618, Nov./Dec. 2000.
18. A. M. EL-Refaie and T. M. Jahns, "Comparison of various types of synchronous PM machines for flux weakening applications", *Proc. IEEE-IAS Annu. Meeting*, 2005-Oct.
19. T. A. Lipo, Introduction to AC Machine Design, WI, Madison:Wisconsin Power Electron. Res. Center, Univ. of Wisconsin,, 1996.
20. J. R. Hendershot Jr. and T. J. E. Miller, Design of Brushless Permanent-Magnet Motors, U.K., Oxford:Clarendon, 1994.
21. Z. Q. Zhu, D. Howe, E. Bolte and B. Ackermann, "Instantaneous magnetic field distribution in brushless permanent magnet DC motors Part IV: Magnetic field on load", *IEEE Trans. Magn.*, vol. 29, no. 1, pp. 152-158, Jan. 1993.
22. Z. Q. Zhu and D. Howe, "Influence of design parameters on cogging torque in permanent magnet machines", *IEEE Trans. Energy Convers.*, vol. 15, no. 4, pp. 407-412, Dec. 2000.